

# Stable Routing and Control System Requirements for Lunar Optical Communication Networks

Antoine D. Goldman\*

*Georgia Institute of Technology, Atlanta, GA, 30332*

Jeffrey McNabb† and Dimitri N. Mavris‡

*Georgia Institute of Technology, Atlanta, GA, 30332*

**Future lunar missions will require high-capacity, delay-intolerant communication networks between the Moon and Earth, pushing the need for optical satellite constellations. This study challenges the assumption of perfect line-of-sight communication by accounting for the physical limitations of satellite control systems required to maintain optical links. A routing strategy is proposed that prioritizes stable, longer lasting paths over traditional shortest path solutions, reducing the frequency of satellite slews. A time-varying graph-based framework is used to compare routing methods and estimate the resulting angular velocity and torque requirements imposed to the spacecraft. Results suggests that the stability-aware routing method can reduce the number of reorientation events and lower average control torque requirements, despite a moderate increase in path length. These findings offer a more physically grounded perspective on the feasibility and sustainability of large-scale cislunar optical networks.**

## I. Introduction

As space agencies and commercial entities prepare for long-duration crewed missions to the Moon, the demand for high-capacity, high-bandwidth, and reliable communication infrastructure between Earth and the lunar surface has never been greater. Next-generation use cases – such as real-time communication with lunar crews, remote control of robotic systems, and Earth-based AI assistance – require delay-intolerant and data-intensive architectures that exceed the capabilities of current systems.

Meeting these requirements necessitates a shift away from traditional radio frequency (RF) communications toward optical systems, which offer significantly higher data rates, lower power consumption, enhanced security, and greater flexibility [1]. However, the adoption of optical communication introduces a new challenge: these systems demand extremely precise pointing and tracking. Due to the narrow beam width of optical links, maintaining a stable line-of-sight (LoS) between communication terminals often requires arcsecond- or microradian-level accuracy [2].

This project investigates the impact of satellite attitude control constraints on the feasibility and sustainability of cislunar optical communication networks. Modern satellite control systems, such as reaction wheels and control moment gyroscopes (CMGs), are subject to actuation limits and risk saturation when exposed to frequent or abrupt reorientation maneuvers.

Conventional routing frameworks typically neglect these physical limitations. To address this, the present study introduces a physically grounded routing strategy that considers both communication performance and the feasibility of satellite pointing. In contrast to idealized shortest-path routing approaches, the proposed method evaluates how dynamic network topology and routing dynamics translate into attitude control demands. The analysis includes a quantitative estimation of the angular velocity and torque required to sustain stable optical links across the Earth–Moon communication environment.

## II. Motivation & Background

DEVELOPING a realistic routing strategy for future cislunar optical communication networks requires an understanding of both prior system-level design assumptions and the physical constraints imposed by satellite attitude dynamics.

\*Graduate Research Assistant, Aerospace Systems Design Laboratory

†Research Engineer II, Aerospace Systems Design Laboratory, and AIAA Member

‡Georgia Tech Distinguished Regents Professor and Director of ASDL, AIAA Fellow

## A. Previous Work

This study expands ongoing efforts in the System-of-Systems design of a next-generation cislunar optical network capable of supporting uninterrupted, high-bandwidth communication between Earth and the Moon.\* That work aims to stress-test network architecture, throughput, and resilience [3].

In the initial study, network architectures were modeled using deterministic orbital mechanics, with inter-node connectivity represented as a sequence of time-evolving graphs. Key performance metrics included average path latency, redundancy, and overall network robustness. These metrics were evaluated under the simplifying assumption that any LoS between nodes enabled perfect, instantaneous, and lossless optical communication.

The present work revisits this assumption by introducing a layer of physical reality to constellation-level communication design.

## B. Satellite Control Constraints and Routing

While the assumption that an existing LoS between two nodes enables instantaneous optical communication allows for rapid design-space exploration, it fails to reflect the physical realities of satellite-based optical networks. Unlike terrestrial digital networks – where latency is primarily driven by data processing – optical satellite constellations must also account for the mechanical latency associated with reorienting the spacecraft to establish and maintain precise optical links [4].

Establishing or switching an optical link typically requires sub-arcsecond pointing accuracy [5], achieved through onboard attitude control systems such as reaction wheels or CMGs. These actuators are subject to physical limitations, momentum buildup, and eventual saturation [6]. Frequent slewing between targets can overwhelm the control system, leading to degraded performance or the need for momentum desaturation maneuvers.

These maneuvers introduce their own operational costs. In systems relying on thrusters or reaction control systems (RCS), desaturation burns consume limited onboard propellant, directly impacting the satellite’s operational lifetime and long-term stability. As a result, routing strategies that reduce the frequency or intensity of attitude adjustments can significantly improve the sustainability of optical communication networks.

This raises a critical question: **How can routing strategies account for the physical cost of establishing and maintaining optical links?** Rather than computing the optimal path based solely on instantaneous connectivity, routing methods must consider the temporal evolution of the network and the control workload incurred by each path. The required slews for each link, the momentum buildup they induce, and the overall attitude control workload introduce new trade-offs when selecting a feasible communication path. Routes must therefore minimize more than just distance or latency as they must also minimize attitude maneuver frequency and burden over time.

This study addresses that gap by proposing a control-aware routing framework for cislunar optical networks by favoring routing strategies that prioritize stability, preferring longer-lasting paths over those that minimize distance alone.

By explicitly modeling the impact of routing on satellite control system demand, this work bridges the gap between high-level network architecture and low-level subsystem feasibility. The outcome is a more physically grounded methodology for evaluating and designing resilient, sustainable cislunar communication infrastructures.

## III. Methodology

THIS study builds upon the modeling & simulation and assessment of a cislunar optical network using a deterministic orbital modeling and graph-based analysis framework, see Fig. 1.

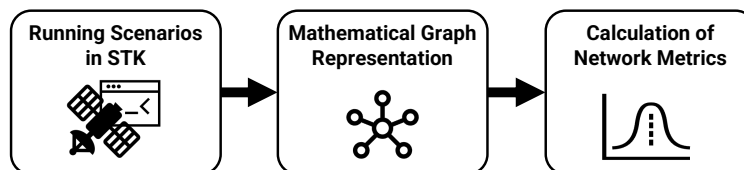


Fig. 1 Modeling & Simulation Framework for the assessment of optical networks.

The methodology comprises of three primary components:

\*A parallel submission detailing the broader System-of-Systems study is currently under review for AIAA SciTech 2026.

- Modeling the satellite network and determining optical access opportunities
- Developing a control-aware routing strategy that challenges conventional shortest-path selection
- Deriving satellite attitude control requirements resulting from the selected routing approach

A baseline network architecture is selected to benchmark the methodology and evaluate trade-offs between routing performance and control feasibility. This architecture ensures full end-to-end connectivity between the lunar surface and Earth.

The modeled network includes:

- **Six Medium-Earth Orbit (MEO)** satellites forming the Earth-side relay layer
- **Two Near-Rectilinear Halo Orbit (NRHO)** satellites operating as the lunar relay layer
- **Six Optical Ground Stations (OGS)** located across the United States and Europe:
  - NASA OGS 1, NASA OGS 2, ESA OGS Tenerife, ESA OGS Almería, ESA OGS Nemea, and ASA OGS Teranet
- **A lunar communication endpoint** located at Nobile Rime 2, a candidate Artemis III landing site [7]

To demonstrate the routing framework and quantify control system implications, the scenario is propagated over a 24-hour period starting on **20 July 2027 at 11:01 UTC**. During this window, access reports and satellite ephemerides are generated to construct the dynamic graph model and evaluate routing decisions over time.

### A. Modeling the Network and Optical Access

The satellite constellation is modeled using **Ansys Systems Toolkit (STK)**, see Fig. 2, with time-accurate orbital propagation and pairwise access computations. Each node in the network (lunar surface, lunar relays, Earth relays, and optical ground stations) is defined as an STK object with assigned ephemerides and communication constraints.

Pairwise **optical access reports** are generated for all relevant node pairs.

These reports provide time-dependent visibility and orientation metrics, including:

- Start and end times of link availability
- Range between nodes at each timestep
- Azimuth and elevation angles, along with their corresponding rates, at each timestep
- Position and velocity vectors of the source node in the Earth-Centered Inertial (ECI) frame at each timestep

These access reports are discretized into fixed time intervals and used to construct a time series of directed graphs, see Fig. 3. In this dynamic graph representation, nodes correspond to satellites or ground terminals, and edges represent viable optical links available at that timestep.

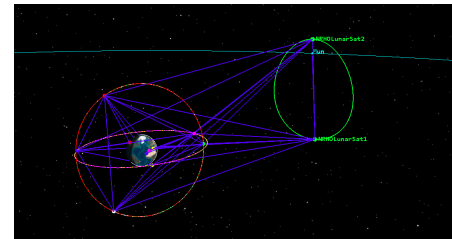


**Fig. 2 STK Visualization of the Baseline Constellation**

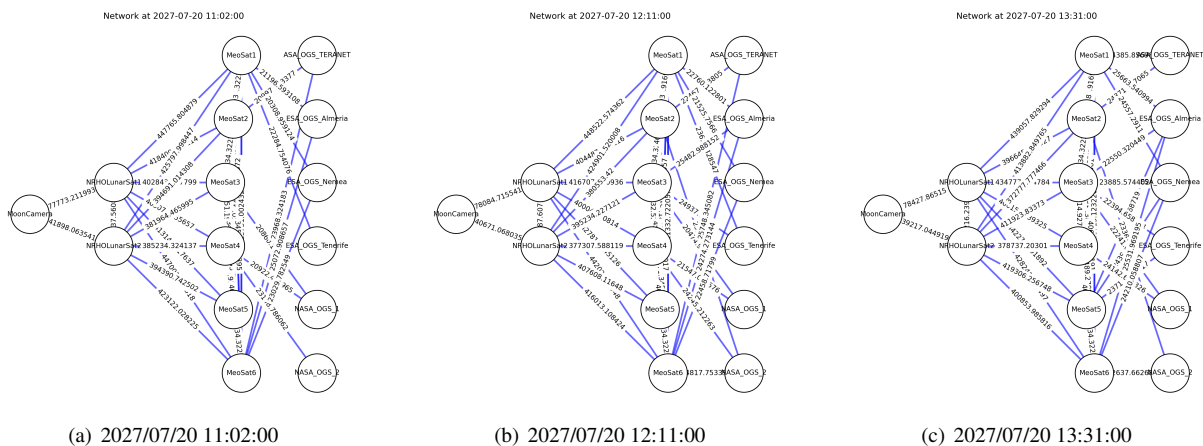


**Fig. 3 Graph Snapshots at Selected Time Steps**

This dynamic graph formulation enables time-aware routing strategies to be tested over the evolving network topology, capturing both orbital dynamics and line-of-sight availability over time.

## B. Routing Strategy Development

Departing from the initial shortest-path routing logic, this study introduces a routing strategy that prioritizes link stability to reduce satellite reorientation frequency [8]. Rather than considering each timestep independently, the proposed method seeks paths that remain stable across multiple consecutive timesteps, thus minimizing the frequency of satellite slews (i.e., attitude reorientations necessary for optical communication).

The routing algorithm operates on a time-varying directed graph  $G(t)$ , where each snapshot represents the network of viable optical links at time  $t$ . The objective is to compute a path sequence  $P(t)$  from a source node  $s$  to a destination node  $d$  (e.g., Earth OGS), while minimizing the total number of reorientation events throughout the entire scenario [9].

### Formal Mathematical Definition

Let  $G(t) = (N, E(t))$  represent the directed graph at timestep  $t$ , where  $N$  is the set of network nodes and  $E(t)$  the set of edges active at time  $t$ .

A valid communication path at time  $t$  is defined as:

$$P(t) = [n_1, n_2, \dots, n_k], \quad \text{with } n_1 = s, n_k = d \quad (1)$$

Given a sequence of discrete timesteps  $T = \{t_1, t_2, \dots, t_m\}$ , the problem becomes one of finding a sequence  $\{P(t)\}_{t \in T}$  that minimizes the total number of reorientations (or *slews*) across the full time interval.

A **slew event** at timestep  $t_i$  is defined as occurring when a node  $n \in N \setminus \{d\}$  changes its next-hop neighbor relative to timestep  $t_{i-1}$ . This can be expressed using the indicator function:

$$X_{n,i} = \begin{cases} 1, & \text{if the next-hop of } n \text{ differs between } P(t_i) \text{ and } P(t_{i-1}) \\ 0, & \text{otherwise} \end{cases} \quad (2)$$

Thus, the routing objective is formulated as:

$$\text{Minimize } \sum_{i=2}^m \sum_{n \in N \setminus \{d\}} X_{n,i} \quad (3)$$

Subject to the feasibility constraints that each path  $P(t)$  must satisfy:

$$(n_j, n_{j+1}) \in E(t), \quad \forall j = 1, 2, \dots, k-1, \quad \forall t \in T \quad (4)$$

While this formulation assumes uniform cost for all reorientations, regardless of the magnitude of the required attitude change, it serves as a foundational model for assessing attitude-aware routing performance.

### Dynamic Programming Framework

To solve this multi-stage optimization problem, a Dynamic Programming (DP) approach is employed [10]. The algorithm constructs the path sequence iteratively, choosing for each timestep the path that yields the minimum cumulative slew cost based on the prior decision. Each state corresponds to a valid path  $P(t)$ , and transitions between states corresponds to a cost equal to the number of slews between successive paths.

Algorithm 1 formalizes the DP-based routing logic

---

**Algorithm 1** DP-Based Stable Routing Algorithm

---

```
1: Input: Graphs  $G[t]$ , ordered timesteps  $T$ , source nodes  $s$ , destination nodes  $d$ 
2: Output: Optimal sequence of paths  $\text{BestPath}[t]$  minimizing total reorientations
3:
4: for each timestep  $t \in T$  do                                     ▶ Initialize data structures
5:   Compute  $\text{FeasiblePaths}[t]$  between  $s$  and  $d$  in  $G[t]$            ▶ Subject to hop limit  $K$ 
6: end for
7: Initialize  $\text{DP\_Cost}[\text{path at } t] \leftarrow \infty$  for all feasible paths
8: Initialize  $\text{DP\_Trace}[\text{path at } t] \leftarrow \text{None}$                  ▶ Traceback structure
9:
10: for each path  $p \in \text{FeasiblePaths}[t_0]$  do
11:   Set  $\text{DP\_Cost}[p, t_0] \leftarrow 0$                                ▶ No initial slew
12: end for
13:
14: for each timestep  $t_i \in T$  do                                   ▶ DP iteration over timesteps
15:   for each  $\text{current\_path} \in \text{FeasiblePaths}[t_i]$  do
16:      $\text{min\_cost} \leftarrow \infty$                                    ▶ Initialization
17:
18:     for each  $\text{previous\_path} \in \text{FeasiblePaths}[t_{i-1}]$  do
19:        $\text{slew\_count} \leftarrow \text{CountSlews}(\text{previous\_path}, \text{current\_path})$ 
20:        $\text{total\_cost} \leftarrow \text{DP\_Cost}[\text{previous\_path}, t_{i-1}] + \text{slew\_count}$ 
21:       if  $\text{total\_cost} < \text{min\_cost}$  then
22:          $\text{min\_cost} \leftarrow \text{total\_cost}$ 
23:          $\text{DP\_Trace}[\text{current\_path}, t_i] \leftarrow \text{previous\_path}$ 
24:       end if
25:     end for
26:      $\text{DP\_Cost}[\text{current\_path}, t_i] \leftarrow \text{min\_cost}$ 
27:   end for
28: end for
29:
30: Backtrack to recover optimal path sequence
31:  $\text{min\_final\_cost} \leftarrow \infty$ 
32:  $\text{best\_final\_path} \leftarrow \text{None}$ 
33: for each path  $p \in \text{FeasiblePaths}[t_{end}]$  do                 ▶ Calling Traceback structure to obtain best path sequence
34:   if  $\text{DP\_Cost}[p, t_{end}] < \text{min\_final\_cost}$  then
35:      $\text{best\_final\_path} \leftarrow p$ 
36:   end if
37: end for
38:
39:  $\text{BestPath}[t_{end}] \leftarrow \text{best\_final\_path}$ 
40: for each timestep  $t_i \in T[1 : m, -1]$  do                   ▶ Backtrack (in reverse) to reconstruct optimal path sequence
41:    $\text{BestPath}[t_i] \leftarrow \text{DP\_Trace}[\text{BestPath}[t_{i+1}], t_{i+1}]$ 
42: end for
43:
44: return  $\text{BestPath}$                                              ▶ For each time  $t$ 
```

---

With the function  $\text{CountSlews}()$  used above, defined in Equation 2 below:

---

**Algorithm 2** Counting Satellite Reorientations Between Paths

---

```
1: function COUNTSLEWS(previous_path, current_path)
2:   slew_count  $\leftarrow$  0 ▷ Initialization
3:
4:   for each node  $n \in$  current_path (excluding  $d$ ) do
5:     next_hop_current  $\leftarrow$  node after  $n$  in current_path ▷ Node immediately following  $n$  in current path
6:
7:     if  $n \in$  previous_path then
8:       next_hop_previous  $\leftarrow$  node after  $n$  in previous_path
9:       if next_hop_previous  $\neq$  next_hop_current then
10:        slew_count  $\leftarrow$  slew_count + 1
11:      end if
12:    else
13:      slew_count  $\leftarrow$  slew_count + 1 ▷ Node newly included in path assumed to count as a slew
14:    end if
15:  end for
16:
17:  Return slew_count
18: end function
```

---

This routing strategy represents a shift from conventional shortest-path methods by introducing a temporal component to the optimization. Rather than recalculating the shortest route at each timestep independently, the algorithm seeks to reduce total maneuvering by favoring path continuity over time.

While the current implementation applies uniform cost to each slew, future improvements could involve weighting each reorientation based on the angular difference, or the required slew rate to follow a LoS. This would allow an even more physically accurate modeling of satellite control requirements in large-scale networks.

### C. Deriving Satellite Control Requirements

Once routing sequences are determined, the required satellite attitude rates are estimated from the angular motion of the optical LoS. STK provides azimuth and elevation rates, which describe the angular tracking required between a transmitting satellite and its target. These are defined relative to the **Vehicle Velocity, Local Horizontal (VVLH)** frame. To derive satellite control requirements, these rates are translated into body-frame angular velocities via coordinate transformation and the use of the transport theorem [11, 12]. To perform this analysis, several reference frames must first be clearly defined. The coordinate systems involved are shown in Fig. 4.

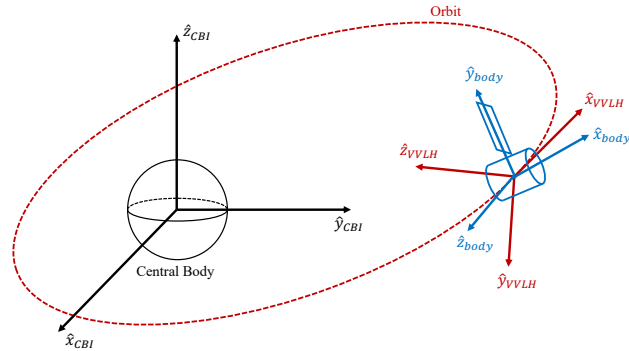


**Fig. 4** Reference frames used for angular velocity estimation.

The **VVLH** reference frame, as defined in STK, is oriented with respect to the ECI frame:

- $\hat{x}_{VVLH}$ : aligned with the satellite's instantaneous velocity vector ( $\hat{v}$ ),
- $\hat{z}_{VVLH}$ : directed toward the geocentric nadir ( $-\hat{r}$ ),
- $\hat{y}_{VVLH}$ : completes the right-handed triad ( $\hat{z}_{VVLH} \times \hat{x}_{VVLH}$ ).

In this frame, azimuth ( $\alpha$ ) and elevation ( $\epsilon$ ) angles define the LoS vector  $\hat{u}$  from the satellite to the communication target. This geometry is illustrated in Fig. 5, following the angle definitions:

- Azimuth ( $\alpha$ ): angle measured from the velocity vector ( $\hat{x}_{\text{VVLH}}$ ) toward  $\hat{y}_{\text{VVLH}}$  in the local horizontal plane,
- Elevation ( $\epsilon$ ): angle measured from the local horizontal plane towards  $-\hat{z}_{\text{VVLH}}$  (downward direction).

The satellite body reference frame orientation relative to the VVLH frame can be described using a standard yaw-pitch-roll Euler angle sequence (3-2-1):

$$\mathcal{F}_{\text{VVLH}} \xrightarrow{R_3(\psi)} \mathcal{F}_1 \xrightarrow{R_2(\theta)} \mathcal{F}_2 \xrightarrow{R_1(\phi)} \mathcal{F}_{\text{body}}$$

For simplicity, it is assumed that the optical communication system is rigidly mounted on the satellite body, with the communication axis perfectly aligned with the body's x-axis. Thus implying:

$$\hat{x}_{\text{body}} \equiv \hat{u}, \quad \text{with} \quad \psi = \alpha, \quad \theta = \epsilon, \quad \phi = 0$$

The composite rotation matrix from VVLH to body frame then becomes:

$$\mathbf{R}_{\text{body/VVLH}} = \begin{pmatrix} \cos \epsilon \cos \alpha & \cos \epsilon \sin \alpha & -\sin \epsilon \\ -\sin \alpha & \cos \alpha & 0 \\ \sin \epsilon \cos \alpha & \sin \epsilon \sin \alpha & \cos \epsilon \end{pmatrix} \quad (5)$$

Using Equation 5, the LoS vector  $\hat{u}$  expressed in the VVLH frame can thus be represented as:

$$\hat{u}_{\text{VVLH}} = \mathbf{R}_{\text{VVLH/body}} \hat{u} = \begin{pmatrix} \cos \alpha \cos \epsilon \\ \sin \alpha \cos \epsilon \\ -\sin \epsilon \end{pmatrix}_{\text{VVLH}}, \quad \text{with} \quad \hat{u} = \begin{pmatrix} 1 \\ 0 \\ 0 \end{pmatrix}_{\text{body}} \quad (6)$$

The rate of change of this LoS vector in the VVLH frame can be obtained directly by differentiating the above equation with respect to time:

$$\left. \frac{d\hat{u}}{dt} \right|_{\text{VVLH}} = \frac{\partial \hat{u}}{\partial \alpha} \dot{\alpha} + \frac{\partial \hat{u}}{\partial \epsilon} \dot{\epsilon} \Rightarrow \left. \frac{d\hat{u}}{dt} \right|_{\text{VVLH}}^{\text{VVLH}} = \hat{u}_{\text{VVLH}}^{\text{VVLH}} = \begin{pmatrix} -\sin(\alpha) \cos(\epsilon) \dot{\alpha} - \cos(\alpha) \sin(\epsilon) \dot{\epsilon} \\ \cos(\alpha) \cos(\epsilon) \dot{\alpha} - \sin(\alpha) \sin(\epsilon) \dot{\epsilon} \\ -\cos(\epsilon) \dot{\epsilon} \end{pmatrix}_{\text{VVLH}} \quad (7)$$

The rotation rate of the body frame with respect to the VVLH frame ( $\bar{\omega}^{\text{body/VVLH}}$ ) is computed using the transport theorem:

$$\left. \frac{d\hat{u}}{dt} \right|_{\text{VVLH}}^{\text{VVLH}} = \left. \frac{d\hat{u}}{dt} \right|_{\text{body}}^{\text{body}} + \bar{\omega}^{\text{body/VVLH}} \times \hat{u} \quad (8)$$

Given the assumption that the vector  $\hat{u}$  is fixed in the body frame,  $\left. \frac{d\hat{u}}{dt} \right|_{\text{body}}^{\text{body}} = 0$ , Equation (8) simplifies to:

$$\bar{\omega}^{\text{body/VVLH}} \times \hat{u} = \left. \frac{d\hat{u}}{dt} \right|_{\text{VVLH}}^{\text{VVLH}} \quad (9)$$

The attitude rate of the body frame with reference to the VVLH frame  $\bar{\omega}^{\text{body/VVLH}} = (P_V \ Q_V \ R_V)^T_{\text{VVLH}}$  is then solved in the VVLH frame from the previously computed  $\hat{u}_{\text{VVLH}}$  and  $\hat{u}_{\text{VVLH}}^{\text{VVLH}}$ . These quantities only depend on the azimuth and elevation angles and rates of the satellite.

Using the skew-symmetric matrix operation, in the VVLH frame:

$$\tilde{\mathbf{u}}_{\text{VVLH}}^T \bar{\omega}_{\text{VVLH}}^{\text{body/VVLH}} = \hat{u}_{\text{VVLH}}^{\text{VVLH}}, \quad \text{with} \quad \tilde{\mathbf{u}} = \begin{pmatrix} 0 & -\sin \epsilon & \sin \alpha \cos \epsilon \\ \sin \epsilon & 0 & -\cos \alpha \cos \epsilon \\ -\sin \alpha \cos \epsilon & \cos \alpha \cos \epsilon & 0 \end{pmatrix}, \quad \text{and} \quad \tilde{\mathbf{u}}_{\text{VVLH}}^T = -\tilde{\mathbf{u}}_{\text{VVLH}} \quad (10)$$

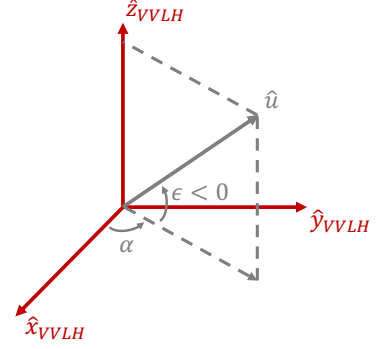


**Fig. 5 Definition of Azimuth and Elevation in the VVLH frame.**

$$\text{Thus, } \bar{\omega}_{\text{VVLH}}^{\text{body/VVLH}} = \begin{pmatrix} P_V \\ Q_V \\ R_V \end{pmatrix}_{\text{VVLH}} = -\tilde{\mathbf{u}}_{\text{VVLH}}^{-1} \dot{\hat{\mathbf{u}}}_{\text{VVLH}}^{\text{VVLH}} \quad (11)$$

The rotation rate of the VVLH frame with respect to the inertial (ECI) frame can be computed from orbital position ( $\bar{\mathbf{r}}$ ) and velocity ( $\bar{\mathbf{v}}$ ) vectors [13]:

$$\bar{\omega}^{\text{VVLH/ECI}} = \frac{\bar{\mathbf{r}} \times \bar{\mathbf{v}}}{\|\bar{\mathbf{r}}\|^2} \quad (12)$$

The total rotation rate of the satellite body frame with respect to the inertial frame (ECI) is given by combining these two rotation rates:

$$\bar{\omega}^{\text{body}} = \bar{\omega}^{\text{body/VVLH}} + \bar{\omega}^{\text{VVLH/ECI}} \quad (13)$$

Expressed explicitly in the body frame using the definition of the VVLH reference frame, Equation (13) becomes:

$$\bar{\omega}_{\text{body}}^{\text{body}} = \begin{pmatrix} \omega_x \\ \omega_y \\ \omega_z \end{pmatrix}_{\text{body}} = \mathbf{R}_{\text{body/VVLH}} \left( \bar{\omega}_{\text{VVLH}}^{\text{body/VVLH}} + \bar{\omega}_{\text{VVLH}}^{\text{VVLH/ECI}} \right) \quad (14)$$

With  $\bar{\omega}_{\text{VVLH}}^{\text{VVLH/ECI}}$  obtained from the definition of the  $\hat{x}_{\text{VVLH}}$ ,  $\hat{y}_{\text{VVLH}}$ , and  $\hat{z}_{\text{VVLH}}$  vectors in the ECI frame:

$$\bar{\omega}_{\text{VVLH}}^{\text{VVLH/ECI}} = \mathbf{R}_{\text{VVLH/ECI}} \bar{\omega}_{\text{ECI}}^{\text{VVLH/ECI}}, \text{ with } \mathbf{R}_{\text{ECI/VVLH}} = \begin{pmatrix} \hat{x}_{\text{VVLH}} & \hat{y}_{\text{VVLH}} & \hat{z}_{\text{VVLH}} \end{pmatrix}_{\text{ECI}} \quad (15)$$

$$\text{With } \hat{x}_{\text{VVLH}} = \frac{\hat{\mathbf{v}}}{\|\hat{\mathbf{v}}\|}, \hat{z}_{\text{VVLH}} = \frac{-\hat{\mathbf{r}}}{\|\hat{\mathbf{r}}\|}, \text{ and } \hat{y}_{\text{VVLH}} = \hat{z}_{\text{VVLH}} \times \hat{x}_{\text{VVLH}} \quad (16)$$

Together, these equations form the core methodology for determining the required satellite attitude rates based on the routing-induced pointing requirements.

The control torque can then be found by applying Euler's rotational dynamics:

$$\bar{\boldsymbol{\tau}} = \mathbf{I} \cdot \dot{\bar{\boldsymbol{\omega}}} + \bar{\boldsymbol{\omega}} \times (\mathbf{I} \cdot \bar{\boldsymbol{\omega}}) \quad (17)$$

Where:

- $\bar{\boldsymbol{\omega}} = \bar{\omega}^{\text{body}}$  the body angular velocity vector
- $\dot{\bar{\boldsymbol{\omega}}}$  the body angular acceleration vector
- $\mathbf{I}$  the spacecraft moment of inertia tensor (assumed constant in the body frame)
- $\bar{\boldsymbol{\tau}}$  the torque vector in the body frame

This study assumes a simplified model in which the entire satellite body must reorient to point its optical communication terminal rather than relying on an independently steerable gimbal. This approach, while not representative of standard laser communication operations practices serves to provide an order-of-magnitude estimate and establish a foundational framework for further, more detailed analyses.

A representative reference platform for this analysis is the student-built CubeSat *MIST* [14]. Its moment of inertia tensor is assumed to be defined as:

$$\mathbf{I} = \begin{pmatrix} I_x & 0 & 0 \\ 0 & I_y & 0 \\ 0 & 0 & I_z \end{pmatrix}, \text{ with } \begin{cases} I_x = 0.037 \text{ kg} \cdot \text{m}^2 \\ I_y = 0.051 \text{ kg} \cdot \text{m}^2 \\ I_z = 0.021 \text{ kg} \cdot \text{m}^2 \end{cases}$$

This top-down modeling approach enables the estimation of angular velocity and torque requirements directly from the selected network routing and pointing dynamics. It thus provides a physically grounded insight into the feasibility of attitude control for small satellite communication systems.

It is important to note that this type of satellite traditionally used in Low Earth Orbit (LEO) orbit are not usually used in MEO due to the increased radiation exposure and other station-keeping factors. Furthermore, while larger satellites can accommodate more robust control systems, they also inherently require greater control torque for attitude adjustments, presenting additional design and operational challenges.

## IV. Findings

THE proposed stability-aware routing strategy was applied to a baseline constellation configuration consisting of six MEO satellites and two NRHO lunar satellites. The system was evaluated over a 24-hour period beginning on July 20th, 2027 at 11:01 UTC. The performance of this method is assessed relative to a traditional shortest-path approach to quantify both communication effectiveness and satellite control workload.

### A. Routing Performance Comparison

Both routing strategies were applied to the same time-varying network topology derived from STK access reports. The shortest-path algorithm selects the minimum-distance route at each timestep, while the proposed stability-aware method seeks to reduce the total number of reorientations by favoring path continuity over time.

Fig. 6 illustrates the temporal distribution of reorientation events across the day. The shortest-path method induces frequent attitude changes, especially when maintaining connectivity between the Moon and Earth, which increases control system workload and introduces potential *slew*-related latency. In contrast, the stable routing strategy spreads out reorientation events more evenly across the simulation window and significantly reduces their total count.

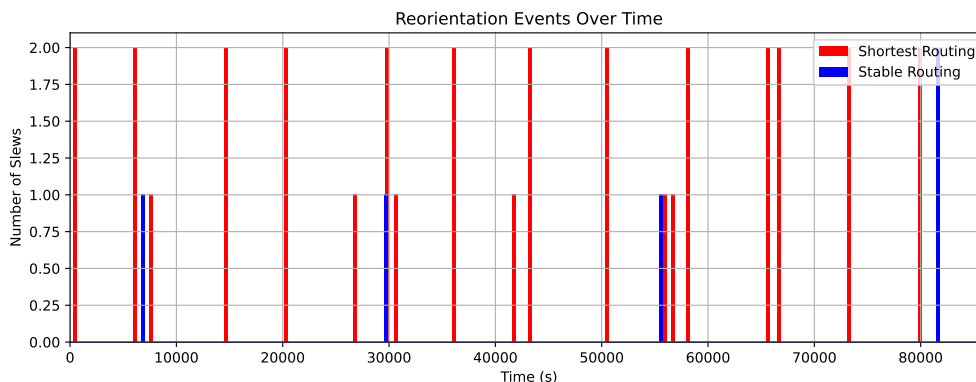


Fig. 6 Comparison of Slew Events Over Time

A side-by-side visualization of each routing strategy at selected timesteps is shown Fig. 7. The stable routing method maintains more persistent paths across time, whereas shortest-path selection exhibits more frequent changes in link configuration.

Quantitative results for each routing method are summarized in Table 1. Although the stability-aware method increases average path distance by approximately 20%, it reduces the number of satellite reorientations from 32 to just 5 over the course of the day. Notably, the average number of node hops remains nearly identical, indicating that increased stability does not come at the cost of topological complexity.

Table 1 Routing Metrics Comparison Across Methods (1-day Timeframe)

Routing Method	Avg. Distance*/ Latency †	Avg. Node Hops	Total Reorientations
Shortest Path	443,263 km / 1.479 s	3.00	32
Stable Routing	531,534 km / 1.773 s	3.08	5

\* Average geometric path length across all evaluated time steps.

† Light-time latency (excluding processing or slew delays).

These results demonstrate the value of incorporating control-aware metrics into routing decisions. Although the stability-aware strategy produces slightly longer paths, it dramatically reduces attitude control burden—lowering the number of reorientations by over 83% with minimal impact on node hops or end-to-end latency. While the current method assumes a uniform cost for reorientations, the framework can be extended to include more detailed constraints such as angular displacement, pointing latency, or required torque, enabling more physically grounded routing strategies.

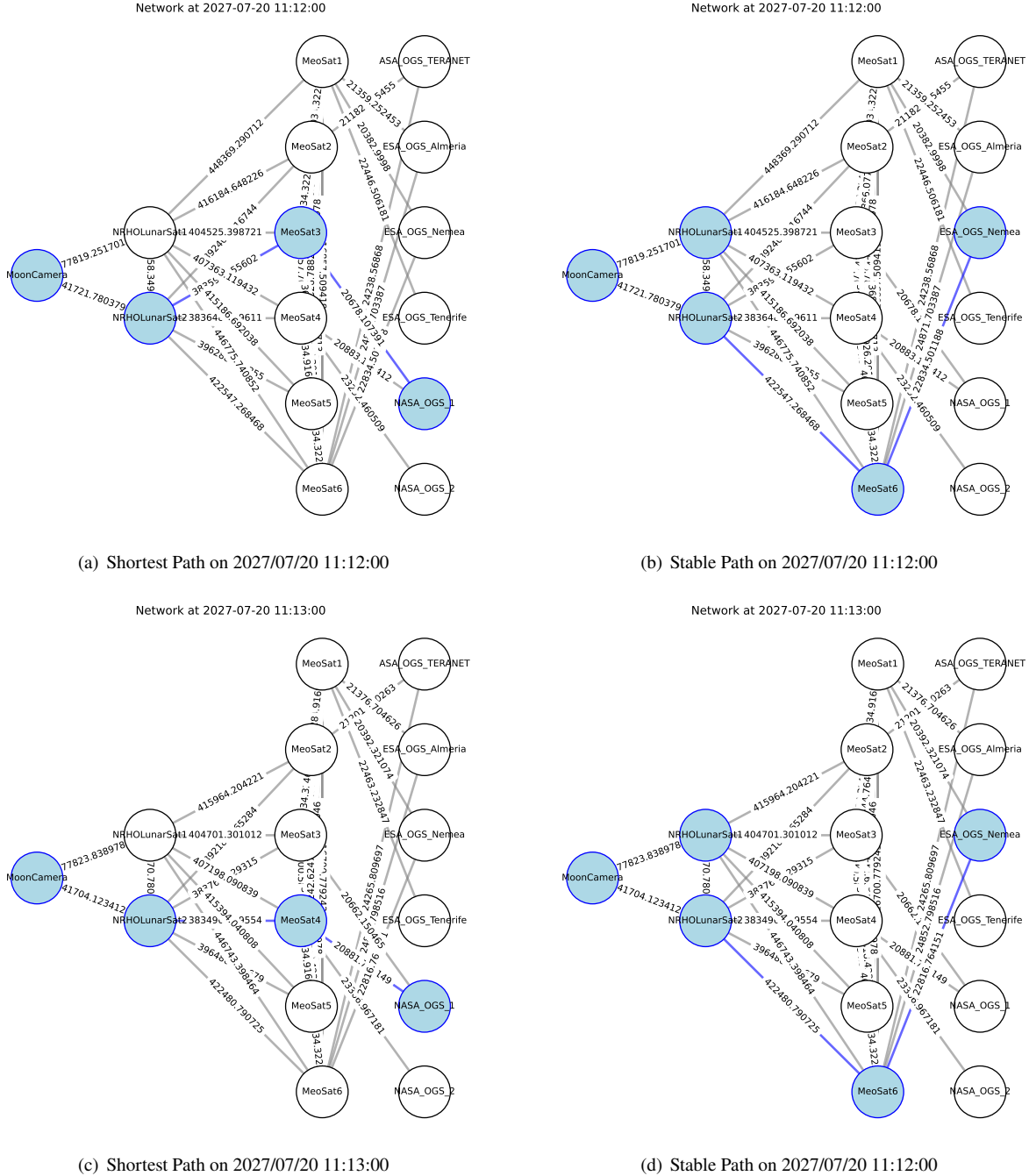


**Fig. 7 Side-by-Side Routing Comparison on the Network Graph**

## B. Attitude Control Implications

The LoS pointing sequences identified through each routing strategy were used to reconstruct the body-frame angular velocity vector  $\bar{\omega}_{\text{body}}$  at each timestep. Angular acceleration was approximated using finite differences, and the required control torque was computed using the rigid-body rotational dynamics developed in Equation 17.

Assuming the moment of inertia matrix of the MIST CubeSat platform, the resulting maximum and average torque values are summarized in Table 2.

Although the stability-aware routing method yields a higher peak angular velocity, it results in a nearly 40% reduction in average torque over the full simulation window. This indicates that smoother, longer-lasting links can reduce the

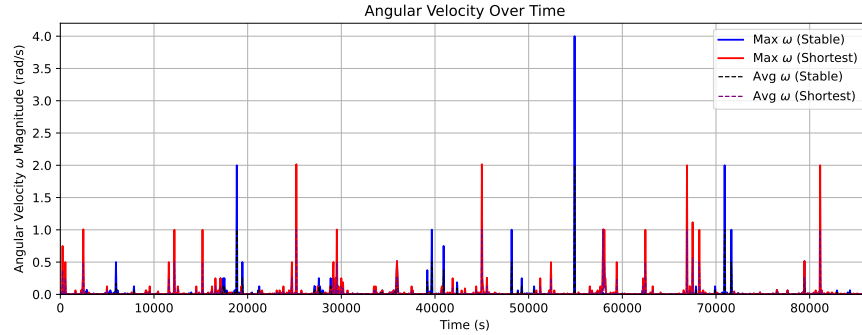
**Table 2 Attitude Control Metrics Comparison (1-day timeframe)**

Routing Method	Max Angular Velocity (rad/s)	Max Torque (mN·m)*	Avg. Torque (mN·m)*
Shortest Path	2.016	2.136	0.0189
Stable Routing	4.000	3.065	0.0117

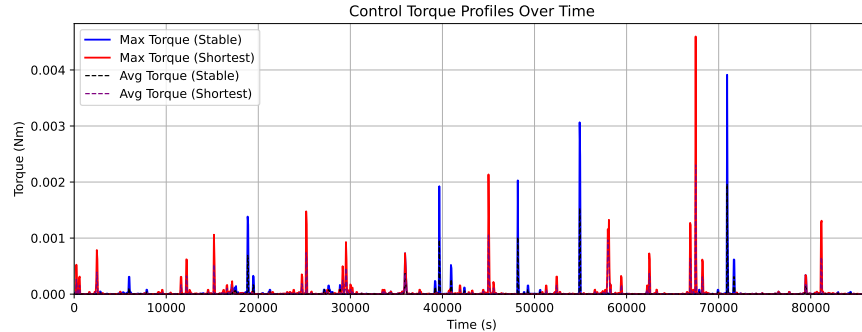
\* Torque values computed using MIST CubeSat inertia matrix.

cumulative workload imposed on attitude actuators even if they require occasional high-speed reorientations. A possible explanation is that longer path lengths correspond to smaller relative angular rates when tracking targets, allowing satellites to maintain stable pointing with minimal control effort over time. However, this benefit comes at the cost of increased precision demands on the optical terminal due to extended link distances.

Fig. 8 illustrates the evolution of instantaneous angular velocity and torque magnitudes over time. Although both methods produce occasional spikes, the average values of the angular velocity  $\omega^{\text{body}}$  and the torque  $\tau$  remain within the capabilities of modern satellite control systems.



(a) Angular Velocity Profile Over Time



(b) Torque Profile Over Time

**Fig. 8 Attitude Control Load Comparison**

These results highlight an opportunity to improve the routing cost function beyond simple slew minimization. Future implementations could integrate metrics such as required angular displacement during a slew, angular velocity, torque, and total path distance into a unified optimization objective. Thus enabling more subsystem-aware optimal routing strategies.

### C. Design Implications

These findings underscore the significance of incorporating control system considerations into network routing decisions for optical communication constellations. While shortest-path routing strategies may optimize link distance or latency in isolation, they can lead to frequent satellite reorientations that place a heavy burden on onboard attitude

control systems.

By contrast, the simple stability-aware routing strategy demonstrates that it is possible to significantly reduce control workload – as measured by average torque and slew events – while maintaining comparable levels of communication performance. This suggests that routing decisions should not be made solely based on geometric efficiency, but must also consider the dynamic behavior and limitations of the spacecraft platform.

The methodology developed here establishes a framework for integrating these subsystem-level constraints into network-level design. It can be generalized to inform early design trade studies for future high-throughput optical missions involving constellations, high-precision pointing, or autonomous operations. Future extensions may incorporate more advanced cost functions, including angular displacement, time-to-slew, or saturation risk, to support control-aware routing strategies for real-time lunar operations.

## V. Conclusion

**T**HIS study introduces a control-aware approach to routing in optical communication networks, emphasizing the trade-offs between communication performance and satellite control effort. By explicitly modeling the attitude reorientation demands required to maintain optical links, a stability-aware routing strategy was developed and compared against traditional shortest-path routing across a representative cislunar communication network.

The results demonstrate that deprioritizing path length in favor of temporal continuity can significantly reduce the number of satellite reorientations, lowering both average torque demands and the operational burden on spacecraft control systems. This was enabled by a dynamic programming algorithm that selects routing paths based on minimizing the number of slews, thereby improving path stability across the simulation timeframe. While the current implementation assumes uniform cost for all reorientations, future extensions may incorporate angular displacement or control torque directly into the cost function to improve physical fidelity and optimality of the path selection.

Furthermore, this study assumed that the entire satellite must rotate to track optical links. In practice, many satellites may use independent actuated optical terminals, which would reduce required body motion. Nonetheless, this assumption provides a valuable upper bound on control workload and establishes a baseline for comparison.

Future work will extend the analysis to include adaptive and predictive routing strategies, more detailed actuator models, and refined cost metrics based on physical motion. These additions will support a more nuanced characterization of the trade-offs between latency, control effort, and link stability in time-evolving satellite networks.

By feeding attitude control requirements – such as angular velocity and torque – back into architecture-level assessments, this methodology offers a pathway to more physically grounded and implementable constellation designs. Ultimately, this work helps bridge the gap between high-level network performance metrics and subsystem-level feasibility, supporting the development of scalable, sustainable optical communication infrastructures for future lunar exploration.

## Acknowledgments

This study was conducted with the support of the Aerospace Systems Design Laboratory (ASDL) at the Georgia Institute of Technology. The authors extend their sincere gratitude to Victor Yang and Alexandre Masset for their guidance and support throughout this research project.

## References

- [1] Williams, W. D., Collins, M., Boroson, D. M., Lesh, J., Biswas, A., Orr, R., Schuchman, L., and Sands, O. S., “RF and Optical Communications: A Comparison of High Data Rate Returns From Deep Space in the 2020 Timeframe,” 12th Ka and Broadband Communications Conference, Naples, Italy, 2007. URL <https://ntrs.nasa.gov/citations/20070017310>.
- [2] Grenfell, P., Aguilar, A., Cahoy, K., and Long, M., “Pointing, acquisition, and tracking for small satellite laser communications,” 32nd Annual AIAA/USU Conference on Small Satellites, 2018. URL <https://digitalcommons.usu.edu/smallsat/2018/a112018/418>.
- [3] Yang, V. A., McNabb, J. T., Balchanos, M. G., and Mavris, D., *Preliminary Approach to Resilient Cislunar Space Domain Awareness Architecture Design*, AIAA SCITECH 2025 Forum, Orlando, 2025. <https://doi.org/10.2514/6.2025-1024>.
- [4] Shi, Y., Yuan, Z., Zhu, X., and Zhu, H., “An Adaptive Routing Algorithm for Inter-Satellite Networks Based on the Combination of Multipath Transmission and Q-Learning,” *Processes*, Vol. 11, No. 1, 2023, p. 167. <https://doi.org/10.3390/pr11010167>.

- [5] Riesing, K. M., Schieler, C. M., Brown, J. J., Chang, J. S., Gilbert, N. C., Horvath, A. J., Petrilli, L. J., Reeve, R. S., Robinson, B. S., Scozzafava, J. J., and Wang, J. P., "Pointing, Acquisition, and Tracking for the TBIRD Cubesat Mission: System Design and Pre-Flight Results," SPIE Photonics West, San Francisco, CA, 2022. URL <https://ntrs.nasa.gov/citations/20210026049>.
- [6] Markley, F. L., and Crassidis, J. L., *Fundamentals of Spacecraft Attitude Determination and Control*, 1<sup>st</sup> ed., Space Technology Library, Springer, New York, NY, 2014. <https://doi.org/10.1007/978-1-4939-0802-8>.
- [7] Peña-Asensio, E., Álvaro Steve Neira-Acosta, and Sánchez-Lozano, J. M., "Evaluating Potential Landing Sites for the Artemis III Mission Using a Multi-Criteria Decision Making Approach," *Acta Astronautica*, Vol. 226, 2025, pp. 469–478. <https://doi.org/10.1016/j.actaastro.2024.10.049>.
- [8] Cao, X., Li, Y., Xiong, X., and Wang, J., "Dynamic Routings in Satellite Networks: An Overview," *Sensors*, Vol. 22, No. 12, 2022. <https://doi.org/10.3390/s22124552>.
- [9] Hanauer, K., Henzinger, M., and Schulz, C., "Recent Advances in Fully Dynamic Graph Algorithms," *1st Symposium on Algorithmic Foundations of Dynamic Networks (SAND 2022)*, Leibniz International Proceedings in Informatics (LIPIcs), Vol. 221, edited by J. Aspnes and O. Michail, Schloss Dagstuhl – Leibniz-Zentrum für Informatik, Dagstuhl, Germany, 2022, pp. 1:1–1:47. <https://doi.org/10.4230/LIPIcs.SAND.2022.1>.
- [10] Bellman, R., *Dynamic Programming*, 6<sup>th</sup> ed., Princeton University Press, 1972.
- [11] Yoon, H., "Pointing system performance analysis for optical inter-satellite communication on CubeSats," Ph.D. thesis, Massachusetts Institute of Technology. Department of Aeronautics and Astronautics., 2017. URL <http://hdl.handle.net/1721.1/113743>.
- [12] Lavezzi, G., Grøtte, M., and Ciarcia, M., "Attitude Control Strategies for an Imaging CubeSat," 2019. <https://doi.org/10.1109/EIT.2019.8833806>.
- [13] Wie, B., *Space Vehicle Dynamics and Control*, 2<sup>nd</sup> ed., AIAA Education Series, American Institute of Aeronautics and Astronautics, 2008. <https://doi.org/10.2514/4.860119>.
- [14] Zhou, J., "Attitude Determination and Control of the CubeSat MIST," 2016. URL <https://urn.kb.se/resolve?urn=urn:nbn:se:kth:diva-203284>.